



# **Evolution of causal relationships under climate change : controls of Net Primary Productivity in the North Altantic Subpolar Gyre**

Germain Bénard<sup>1</sup>, Marion Gehlen<sup>1</sup>, and Mathieu Vrac<sup>1</sup>

<sup>1</sup>Laboratoire des Sciences du Climat et de l'Environnement (LSCE-IPSL), CEA/CNRS/UVSQ, Université Paris-Saclay, Centre d'Etudes de Saclay, Orme des Merisiers, 91191 Gif-sur-Yvette, France

**Correspondence:** Germain Bénard (gbenard.gb@gmail.com)

#### Abstract.

Understanding how climate change affects marine primary productivity requires examining the evolving causal relationships between physical and biogeochemical processes. We applied the PCMCI+ causal discovery algorithm to investigate how the mechanisms controlling Net Primary Productivity (NPP) in the North Atlantic Subpolar Gyre evolve under different climate scenarios across five Earth System Models. Using 100-year sliding windows, we compare causal relationships in future scenarios against pre-industrial conditions, focusing on the roles of mixed layer nutrients, vertical mixing and horizontal transport. Our analysis reveals three main categories of relationship evolution: the emergence of links, the disappearance of links, and changes in link strengths. For example, while the link between stratification and NPP emerges under climate change in CanESM5-CanOE, it strengthens in CMCC-ESM2 and remains stable with moderate to high intensities in other models. At the end of the 21st century, the spread between models regarding the effect of stratification on NPP is reduced compared to preindustrial conditions, suggesting a reduction in inter-model uncertainty. However, the transport and vertical mixing controls on the supply of nutrients to the mixed layer exhibit a more diverse evolution among the ESMs studied. The CMCC-ESM2 model has a strengthening of the relationships between winter vertical mixing and nutrients, while IPSL-CM6A-LR and CanESM5-CanOE show weakening of these relationships. Furthermore, the evolution of the link between nutrient supply to the mixed layer for NPP exhibits a large variability between models. These divergent pathways reveal that the dynamics of nutrients has uncertain evolution between models. Lastly, model-specific dynamics are also observed, such as the strengthening of the link between horizontal transport and the nutrient content of the mixed layer in IPSL-CM6A-LR. Together with the decreasing strength of the vertical mixing/nutrients link, this suggests the presence of compensation mechanisms and a shift from vertical mixing dominance to enhanced horizontal transport control over the course of the scenario. These findings offer mechanistic insights into the dynamics of ESMs, specifically in the evolving relationships between physical and biogeochemical processes that shape the projections of NPP and nutrients. The causality-based approach identifies mechanisms that traditional analyses miss, offering a novel framework for model intercomparison and understanding ecosystem responses to climate change.





# 1 Introduction

Earth System Models (ESMs) are powerful tools for projecting future climate states and understanding complex Earth system interactions (Séférian et al., 2020; Vautard et al., 2021; Tsujino et al., 2020; Ukkola et al., 2020). Although these models have shown considerable skills in simulating historical and present-day dynamics, including ocean physics and marine biogeochemistry, significant uncertainties persist in their projections of future conditions. (Kwiatkowski et al., 2020; Tagliabue et al., 2021; Turnock et al., 2020; Ukkola et al., 2020). These uncertainties stem from two primary sources: the inherent uncertainty in future emission scenarios and the structural differences between models. The latter arise from varying model architectures, spatial resolutions, selections of complex physical and biogeochemical processes and their parameterizations(Bonan and Doney, 2018; Zelinka et al., 2020). In particular, for net marine primary productivity (NPP), the spread between models exceeds the uncertainty based on scenarios (Kwiatkowski et al., 2020) – a pattern that stands in stark contrast to other projected variables such as the sea surface temperature (Bopp et al., 2013; Kwiatkowski et al., 2020). This uncertainty highlights the complexity of physical-biogeochemical interactions in models and calls for an investigation of how these processes are represented across different ESMs.

NPP variability arises from a complex cascade of interactions between atmospheric, physical, and biogeochemical processes. This cascade begins with atmospheric processes, which drive ocean dynamics through heat and momentum exchanges (Large and Yeager, 2012; Bishop et al., 2020), influencing large-scale circulation patterns and local vertical mixing processes(Martinez et al., 2011; Damerell et al., 2020). These physical mechanisms, in turn, govern nutrient availability (Steinhoff et al., 2010; D'Asaro, 2008; Williams et al., 2006) – key determinants of marine primary productivity. Winter vertical mixing is a critical component of this chain. It serves as the primary mechanism for replenishing surface waters with nutrients from deeper layers (D'Asaro, 2008; Williams et al., 2006), thus setting the biogeochemical conditions for vigorous spring blooms characteristic of temperate subpolar regions.

The subpolar North Atlantic emerges as a particularly relevant region for investigating these interconnected processes, hosting highly productive ecosystems characterized by intense spring blooms and pronounced seasonal cycles. This region has its own distinct mode of variability: the North Atlantic Oscillation (NAO) dominates atmospheric variability, driving changes in wind patterns, heat fluxes, and precipitation that directly influence ocean dynamics(Hurrell et al., 2003b; Khatri et al., 2022). The North Atlantic Subpolar Gyre and the North Atlantic Current are key features of the regional circulation. Both play crucial roles in the horizontal transport and mixing of water masses that bring nutrients to the area (Pelegrí et al., 2006). Climate change is already leaving its mark on this system, with documented freshening and cooling trends (Holliday et al., 2020) that have the potential to modify circulation patterns and, consequently, nutrient distributions (Hátún et al., 2017; Tagliabue et al., 2021). Notably, this region exhibits some of the largest inter-model disagreements in NPP projections (Tagliabue et al., 2021). This uncertainty stems not only from differences in the representation of biogeochemical processes but also from varying representations of physical mechanisms that drive nutrient supply and biological productivity. These characteristics make the subpolar North Atlantic an ideal case study for investigating how different models represent the complex chain of interactions leading to NPP variability, and how these representations contribute to uncertainty in future projections.

https://doi.org/10.5194/egusphere-2025-4680 Preprint. Discussion started: 13 November 2025

© Author(s) 2025. CC BY 4.0 License.





Recent observational and modelling studies have highlighted several significant changes in a warming climate. The intensification of upper-ocean stratification, projected to increase by 16-30% globally by 2100 (Fu et al., 2016), emerges as an important driver of change, potentially inhibiting nutrient replenishment during productive periods and consequently affecting bloom dynamics (Behrenfeld et al., 2006; Bopp et al., 2013). Additionally, alterations in ocean circulation patterns are reshaping nutrient transport, with implications for regional productivity (Hátún et al., 2017; Whitt and Jansen, 2020; Williams et al., 2011). However, the representation and relative importance of these mechanisms vary among ESMs (Fu et al., 2016) due to model-specific structural characteristics and parametrizations. Fundamental differences in the representation of physical-biogeochemical interactions may contribute to the large spread in future NPP projections for this region (Tagliabue et al., 2021; Kwiatkowski et al., 2020; Fu et al., 2016). Our study examines the influence of the temporal evolution of vertical mixing and horizontal transport on nutrient availability and the subsequent control of nutrient variability on NPP in the subpolar North Atlantic across 5 ESMs and three emission scenarios (SSP126, SSP245, SSP585).

To disentangle these complex interactions and understand their potential evolutions under climate change, we use a causality-based approach for model intercomparison. The present study builds on Bénard et al. (2025) who explored these interactions in a pre-industrial simulation. By employing the PCMCI+ algorithm (Runge et al., 2019), this methodology enables the identification and quantification of causal relationships between key variables in the climate system. This approach goes beyond traditional correlation-based analyses, allowing us to detect relationships that may persist, emerge, or disappear under different climate change scenarios.

## 2 Data and methods

Our methodological approach consists in analyzing the evolution of causal relationships within a predefined conceptual scheme linking the physical and biogeochemical variables of the Eastern part of the North Atlantic Subpolar Gyre under different climate scenarios. We apply the PCMCI+ algorithm multiple times using a sliding window approach to examine how causal links evolve progressively from pre-industrial conditions to future projections. This strategy allows us to address non-stationarity inherent to climate change scenarios while keeping long enough time periods to detect changes in the system's causal structure.

A brief presentation of PCMCI+ principles is given in the following subsection, followed by the description of the selected variables and our temporal analysis protocol.

# 2.1 PCMCI+

To investigate the causal links among variables, we employ the PCMCI+ method (Runge et al., 2019; Runge, 2020), following the approach detailed in (Bénard et al., 2025). PCMCI+ is a causal discovery algorithm based on Granger causality that identifies both contemporaneous and time-lagged relationships between multiple variables. The algorithm creates a causal graph where nodes represent variables and edges represent causal links, with each link characterized by its lag (0 for contemporaneous relationships) and strength (ranging from -1 for the strongest negative link to 1 for the strongest positive link).





The algorithm proceeds in two main steps: (1) the PC (Peter & Clark) step, which iteratively tests conditional independence between variables to eliminate spurious links and obtain a set of parent variables; and the (2) MCI (Momentary Conditional Independence) step, which tests the influence of more distant variables through the examination of relationships with the explanatory variables of the parents previously identified. For a comprehensive description of the algorithm, including details of the mathematical framework and its implementation, we refer the reader to Runge et al. (2019) and Bénard et al. (2025).

In the following, the maximum lag value is set to T=3 years to investigate lagged interactions within the interval [0,T].

The algorithm uses False Discovery Rate control (Benjamini and Hochberg, 1995) to determine the statistical significance of causal links, rather than relying on a predetermined minimum strength threshold. This significance will be a criteria to characterize emerging links (non-significant links that become significant) or disappearing links (links that become non-significant).

For each PCMCI+ run (i.e., on each sliding window), we record the minimum strength value among all significant links detected. When aggregating multiple causal graphs together (e.g., when averaging causal graphs obtained from n consecutive years), we establish a threshold by calculating the average of these minimum significant strengths across multiple runs.

#### 2.2 Variables selected

100

110

We selected a set of 5 Earth system models: IPSL-CM6A-LR (Boucher et al., 2020), CESM2 (Danabasoglu et al., 2020), CMCC-ESM2 (Lovato et al., 2022), UKESM1-0-LL (Sellar et al., 2019; Yool et al., 2021) and CanESM5-CanOE (Christian et al., 2021; Swart et al., 2019). The biogeochemical models in those ESMs share a similar complexity: they include at least 2 phytoplankton functional types (PFT) with model-specific parameterisations of interactions between PFTs, as well as nutrient limitation of phytoplankton growth. Details on these ESMs are given in the supplementary.

Building upon (Bénard et al., 2025), we focus on the eastern subpolar gyre with a specific set of variables. This region exhibits significant sensitivity to climate change, with a strong spread in projected NPP values (Kwiatkowski et al., 2020; Tagliabue et al., 2021). While (Bénard et al., 2025) established the causal relationships under pre-industrial conditions, here we examine how these relationships evolve under climate change.

The intensity of the spring bloom is the target variable, which is defined by the maximum NPP reached during the bloom. Nutrient availability contributes to controlling the intensity and duration of the spring bloom. We analyze four nutrients: nitrate, silicate, dissolved iron, and phosphate. Deep winter mixing establishes the nutrient inventory in the euphotic zone by entrainment of nutrients from deeper layers. In our analysis, it is represented by the maximum winter mixed layer depth (MLD). Stratification during the bloom inhibits the upward mixing of nutrients which ultimately contributes to limit its intensity and duration. In addition to the vertical processes that inject nutrients at the base of the mixed layer, nutrients are contributed by horizontal advection which is represented by the gyre circulation and transport across a section. This section is selected to capture the intense circulation along the southern boundary of the subpolar gyre in every ESM. Specifically, we aim to quantify the nutrient input from the North Atlantic Current (NAC) branch that feeds into the eastern part of the subpolar gyre. The North Atlantic Oscillation (NAO) acts as the primary atmospheric driver, influencing these physical variables through its control over regional climate variability.



125

150



Variables were processed as time series of annual means from monthly model outputs. For NPP, we focused on the maximum value reached during the spring bloom. To capture the pre-bloom nutrient stock available for the spring bloom, the maximum of nutrient concentrations in the upper 100 m water column reached before bloom initiation is diagnosed. The start of the bloom is determined using a threshold method (Brody et al., 2013), defined as the first month when NPP exceeds the median value plus 5%.

For MLD the maximum value reached during November-April, the period preceding the bloom, is used. The NAO index is computed by identifying persistent high and low pressure zones (Hurrell et al., 2003a) across the North Atlantic and calculating their pressure difference during the bloom period. Gyre strength is quantified using a 7.5 Sverdrup threshold on the barotropic streamfunction integrated over 2000 m depth, averaged from bloom start to peak. Stratification is measured as the density difference between 100 m depth and the sea surface during bloom. All processed variables are centered (zero mean) and scaled (unit standard deviation) before further analysis. For a more detailed version of data processing, we refer to (Bénard et al., 2025).

The transport variable is built to capture the eastward transport originating from the North Atlantic Current (Rossby, 1996). It is calculated as the nutrient transport across a fixed section at 33°W between 46.5°N and 57.5°N. It is calculated over the upper 100 m of the water column for sake of consistency with the depth range used for the analysis of the concentration of nutrients. For each model grid point along the section, transport of nutrients is calculated by multiplying zonal velocities with nutrient concentrations. This refined approach compared to Bénard et al. (2025) allows us to better isolate the contribution of horizontal advection to nutrient availability in the eastern subpolar gyre. This region is of particular relevance in the context of climate change as circulation patterns might evolve.

The graphs of causal relationships will be explored separately for each nutrient (nitrate, dissolved iron, silicate and phosphate). We anticipate that the strength of nutrient-productivity relationships will evolve differently for each nutrient, reflecting changes in limiting factors under climate change.

# 2.3 From Pre-industrial and historical simulations to future scenarios

Historical simulations (1850-2015) combined with three future scenarios (2015-2100) of increasing radiative forcing are analyzed: SSP126 (low), SSP245 (medium), and SSP585 (high) (Riahi et al., 2017). This range of scenarios allows us to investigate the progressive impact of climate change on causal relationships within the physical-biogeochemical system.

A key methodological challenge in this study stems from the non-stationarity inherent to climate change scenarios, which conflicts with the stationarity assumption of PCMCI+ (Runge, 2020). Non-stationarity can affect our analysis through multiple mechanisms: it can invalidate the assumption of stable relationships in linear regressions, alter the underlying distributions that statistical tests rely on, and potentially create spurious partial correlations due to shared anthropogenic forcing trends. To address these challenges, we implement a sliding window approach rather than analyzing the full 250-year period. We apply PCMCI+ to each successive 100-year window, which helps to:

- Reduce the impact of non-stationarity within each analysis window,

https://doi.org/10.5194/egusphere-2025-4680 Preprint. Discussion started: 13 November 2025

© Author(s) 2025. CC BY 4.0 License.



155

160

180



- Enable the investigation of temporal evolution in causal relationships,

Provide a distribution of link strengths for each causal link under different scenarios.

As a reference for the end of the scenario, we focus on the last 35 sliding windows, as more than half of the years in these windows belong to the scenario period, making them most representative of the final scenario state. We examined the performance of PCMCI+ according to the length of time-series with auto-regressive vectors. Our sensitivity analysis (not shown) demonstrated that, although the links discovered are still similar, shorter time series produce higher estimation errors in link strength. This justifies our choice of 100-year windows as a compromise between minimizing non-stationarity effects and maintaining sufficient sample size for robust causal discovery. For comparison with natural variability, we apply the same sliding window approach to the pre-industrial control simulation. This allows us to compare distributions of link strengths between pre-industrial and future scenario runs. The statistical significance of changes is assessed using both the Cramer-von Mises test (Anderson, 1962) for distributional changes and t-tests (Kim, 2015) for shifts in mean values. We also use the pre-industrial range (Minimum and maximum values reached) of strength to characterize emerging and disappearing links. This approach enables us to distinguish climate change-induced alterations in causal relationships from internal variability. Note that for CESM2 we do not have access to compatible simulations for both pre-industrial and future scenarios. Therefore, for this model, we do not compare results to the pre-industrial distribution.

## 3 Results

This section presents selected causal links between physical and biogeochemical variables and their temporal evolution across climate scenarios. First we examine the evolving contribution of nutrient variability to NPP. Next we investigate the changing influence of vertical mixing and advective transport of nutrients to NPP. The analysis relies on the causal graphs obtained from PCMCI+.

The multiple causal graphs obtained by applying the 100-year sliding window enable the comparison between pre-industrial conditions and the historical period. Taking results for CanESM5-CanOE as an example, Figure 1 illustrates a causal graph obtained under pre-industrial conditions and the mean causal graphs representative for each SSP scenario. The latter are derived from the 35 last sliding windows. This figure illustrates the major changes in causal relationships, which can be characterized as:

- Emerging links: relationships becoming significant;
- Disappearing links: relationships becoming non-significant;
- Changes in strength: relationships with mean values significantly different from pre-industrial values sometimes reaching values outside the range of pre-industrial strength.

In the following, we mainly use the CanESM5-CanOE model for illustration. The complete set of causal graphs for all models is available in the **supplementary** materials (Figure S1-S4).





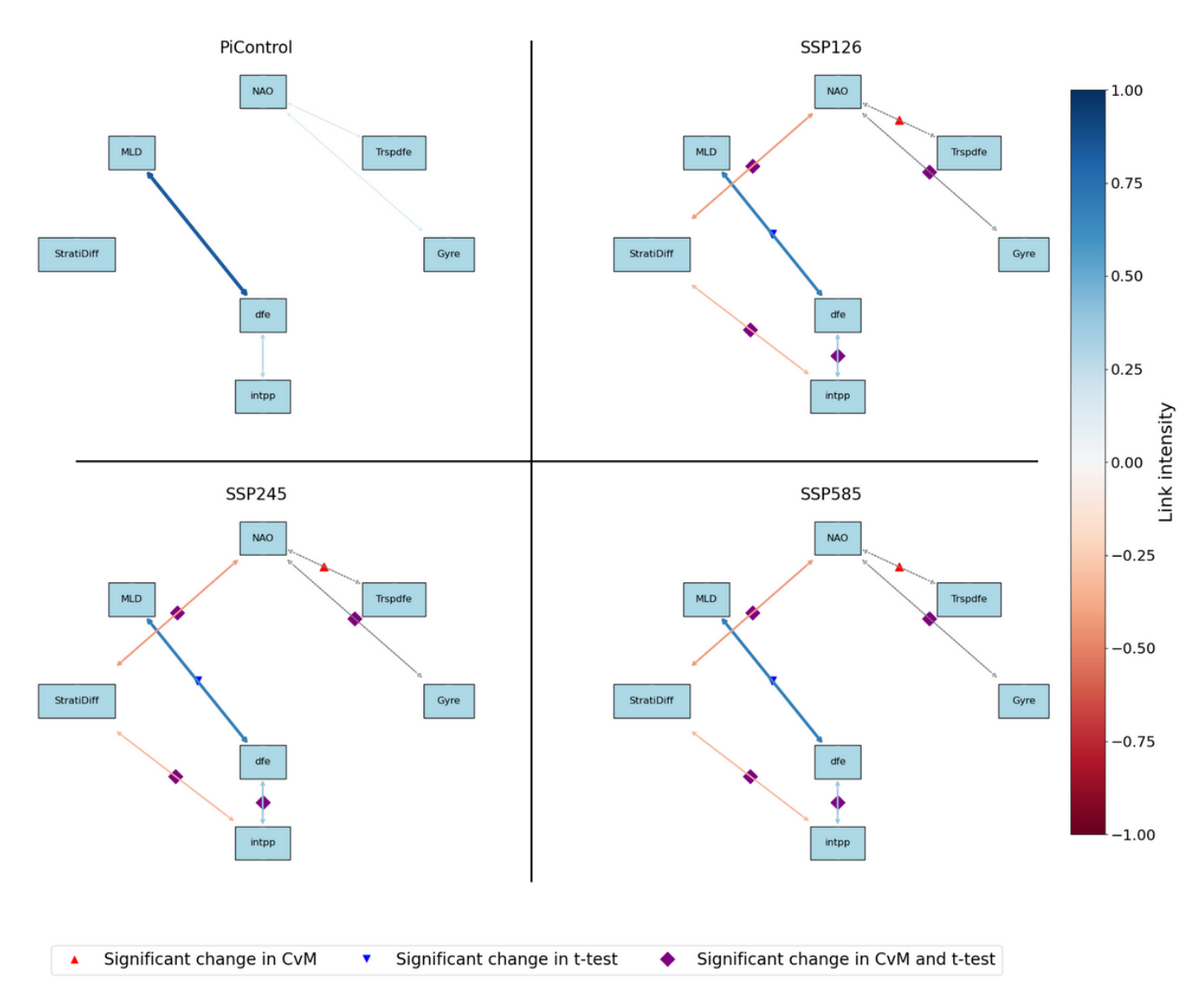


**Figure 1.** Mean causal graph (over the 35 last sliding windows) according to each scenario. The colorbar indicates the intensity of the strength of the link. Only links with a strength above 0.31 (the average minimum significant strength) are displayed. The grey indicates a link that existed in pre-industrial simulation and disappeared under SSP scenario. MLD: Mixed layer Depth; StratiDiff: Stratification; dFe: Iron; intpp: NPP; Gyre: Gyre index; TrspDFe: Iron Transport





# 185 3.1 Evolving role of nutrients

The analysis of causal relationships between nutrients and productivity reveals a diversity of responses to climate change. The complete results for all models are synthesized in Table 1, which presents the trends, the proportion of points outside the pre-industrial distribution, the significativity of the relationships, and their intensity.

Table 1. Summary of nutrient-productivity relationships. Values and trends are given in the order of scenarios SSP126/SSP245/SSP585. Trends are indicated by + (positive), - (negative), 0 (stable), and with doubled signs (++ or --) for strong trends ( $\geq 1 \times 10^{-3}$ ). Bold numbers indicate a high proportion of significant strengths (>30/35 points). "Outside PI" corresponds to the number of points (out of 35) outside the pre-industrial value range. "Sig." counts the number of significant points among the 35 last values. Mean intensity value for the last 35 values are given for each scenario. Missing pre-industrial data for CESM2, Non-Assigned (NA) values for this model for "Outside PI".

| Model         | Nutrient  | Trend    | Outside PI      | Sig.             | Intensity      |
|---------------|-----------|----------|-----------------|------------------|----------------|
| CanESM5-CanOE | Iron      | ++/++/++ | 19/18/0         | 31/35/24         | 0.55/0.55/0.35 |
|               | Nitrate   | ++/++/++ | 33/33/35        | 34/34/35         | 0.55/0.55/0.6  |
| IPSL-CM6A-LR  | Iron      | +/++/0   | 3/ <b>35</b> /0 | 35/35/30         | 0.55/0.65/0.45 |
|               | Nitrate   | -/-/+    | 0/0/29          | 30/35/35         | 0.45/0.55/0.6  |
|               | Silicate  | -/-/++   | 8/6/ <b>35</b>  | 17/29/ <b>35</b> | 0.4/0.5/0.6    |
|               | Phosphate | -/0/++   | 0/0/13          | 26/35/35         | 0.40/0.50/0.65 |
| CMCC-ESM2     | Iron      | //       | 29/1/18         | 0/0/0            | -              |
|               | Nitrate   | 0/0/     | 6/0/12          | 22/27/19         | 0.4/0.45/0.3   |
|               | Silicate  | //       | 11/18/19        | 21/15/14         | 0.35/0.3/0.2   |
|               | Phosphate | 0/0/-    | 3/0/4           | 19/28/19         | 0.40/0.50/0.35 |
|               | Iron      | ++/++/++ | NA              | 0/0/0            | -              |
| CESM2         | Nitrate   | ++/++/+  | NA              | 1/4/0            | -              |
|               | Silicate  | ++/++/+  | NA              | 0/0/0            | -              |
|               | Phosphate | ++/++/++ | NA              | 4/13/0           | -              |
| UKESM1-0-LL   | Iron      | +/+/-    | 0/9/28          | 0/0/0            | -              |
|               | Nitrate   | ++/++/+  | 3/0/0           | 35/35/35         | 0.8/0.8/0.75   |
|               | Silicate  | ++/++/++ | 1/0/0           | 35/35/35         | 0.8/0.8/0.75   |
|               | Phosphate | ++/++/+  | 4/0/0           | 35/35/35         | 0.80/0.80/0.75 |

We analyze the contribution of nutrient variability to projected variability of NPP for four key nutrients: iron, silicate, nitrate and phosphate. Our analysis reveals that the dynamics between these nutrients and productivity varies significantly between different models and even within the same model between different nutrients.

For example, the CanESM5-CanOE model exhibits varying evolutions with time of the link between nitrate, respectively, iron and NPP (silicate and phosphate are not available for this model) between scenarios. The results are shown in Figure 2, where the scatter plots depicting the evolution of strength are flanked by histograms representing the distribution of strength



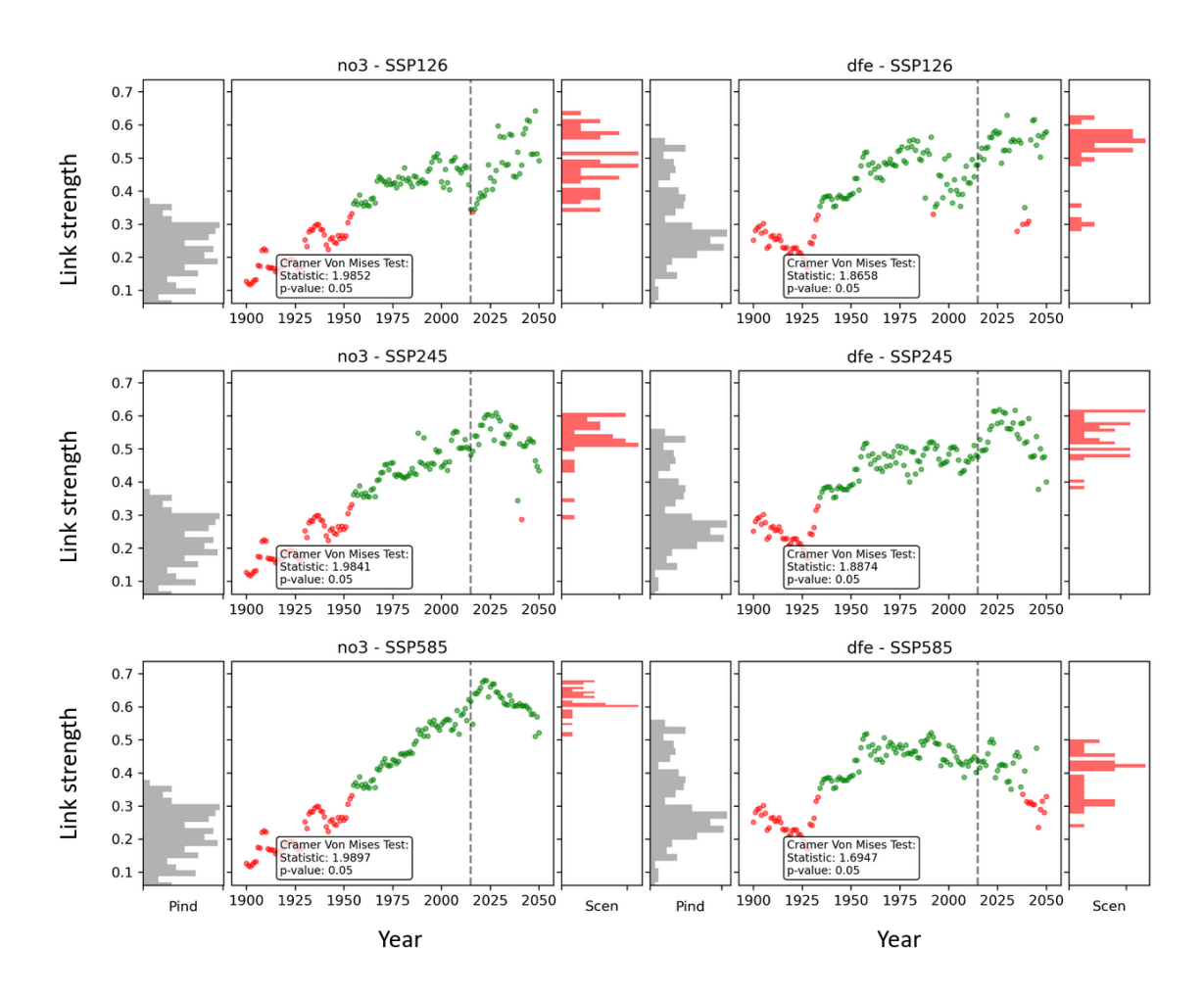


**Figure 2.** Evolution of the link nutrient/net primary productivity for each scenario for CanESM5-CanOE. Each row corresponds to a scenario. The first column corresponds to nitrate and the second one to iron. On the leftmost part of each column, the grey histograms illustrate the strength of the link for a pre-industrial simulation. The scatter plots represent the strength evolution under each scenario, with red indicating non-significant and green indicating significant relationships. Additional red histograms (rightmost part of each column) display the distribution of the relationship strength, based on the last 35 windows of the scenario.



205

210

220

225



under pre-industrial conditions (left) and future scenario (right). The relationship between iron and productivity maintains strength values within the pre-industrial distribution, suggesting relatively stable dynamics. We nevertheless note a positive trend between 1920 to 2030 for SSP126 and SSP245 with a strength of about  $2.2 \times 10^{-3}$  per year. To the contrary, nitrate shows a clear emerging dynamic (starting to be significant in 1960). We observe an increase in strength mostly over the historical period reaching values of approximately 0.6 under climate change scenarios (Table 1). Trends from the start of the simulation to 2020 vary between scenarios, with the weakest trend computed for SSP126 ( $3 \times 10^{-3}$  per year), followed by SSP245 ( $3.7 \times 10^{-3}$  per year), and SSP585 ( $4.4 \times 10^{-3}$  per year). These results suggest that in the CanESM5-CanOE model, nitrate variability is playing an increasingly important role in controlling the variability of NPP.

Changing interactions in response to climate change were also obtained for IPSL-CM6A-LR and CMCC-ESM2. The strength of the link between between nitrate and NPP increased in IPSL-CM6A-LR under SSP585. There is a positive trend of  $3.7 \times 10^{-4}$  per year reaching values outside of the pre-industrial range at approximately 0.6 (Table 1). The link silicate  $\rightarrow$  NPP and phosphate  $\rightarrow$  NPP exhibit even stronger trends of respectively  $1.7 \times 10^{-3}$  and  $1.1 \times 10^{-3}$  per year, also reaching values outside the pre-industrial range of approximately 0.6 for silicate and 0.65 for phosphate (Table 1). For the other scenarios, the strength remains stable. No significant trend is found for the evolution of the link between NPP and iron under SSP585. However, around the year 2000, the strength peaks at 0.65 (outside of the pre-industrial range). The same increase is obtained in response to SSP245 but values remain around 0.65 until the end of the scenario (Table 1).

While a positive trend in strength suggests an increasing contribution of nutrients to the modeled variability of NPP, the inverse is also found. CMCC-ESM2 also has different dynamics in response to SSPs with disappearing links. Considering only the significant links, CMCC-ESM2 stays inside the pre-industrial range. However, when we also look at the non significant links, there is an important decline over the last years for nitrate, phosphate and silicate. Over the period 2020-2050, a negative trend is obtained in all scenarios:  $-1.8 \times 10^{-2}$  to  $-1.4 \times 10^{-2}$  per year for nitrate,  $-2.0 \times 10^{-2}$  to  $-1.7 \times 10^{-2}$  per year for silicate;  $-1.9 \times 10^{-2}$  to  $-1.3 \times 10^{-2}$  per year for phosphate. This relationship is not significant in the last years for each scenario, however, the strength reaches values that are outside the pre-industrial range. A decreasing contribution of nutrients to the control of NPP variability under climate change is a unique feature of CMCC-ESM2 (albeit considering non significant causal links).

Considering the other models, UKESM1-0-LL has unchanged dynamics with values inside the pre-industrial range, but still has a null or positive trend for their strength. Lastly, CESM2 has links that stays mostly non significant.

The results for each nutrient are summarized in table 1.

# 3.2 Evolving role of the vertical mixing

The impact of stratification on productivity varies between models. Some models project unchanged dynamics, while others show evolving relationships under climate change scenarios. The complete results for all models are synthesized in Table 2.

In models with unchanged dynamics, such as UKESM1-0-LL, the link between stratification and NPP remains stable. However, this does not imply that climate change has no impact. For example, under the SSP585 scenario, the intensity of the variable stratification increase with a trend of  $4.9 \times 10^{-3}$  per year, while the variable NPP decreases with a trend of



230

235

240

245

250



 $-2.6 \times 10^{-9}$  mol·m<sup>-2</sup>·s<sup>-1</sup> per year. Dividing these trends by the mean value of each variable to compare them, we obtain very similar normalized trends: 0.013 per year for stratification and -0.012 per year for productivity. Given the strong causal link between the two (approximately -0.7), this close relationship between trends in underlying variables can be expected. The variable trends for all the models are indicated in the supplementary (Figures S5-S9).

While a strong correlation between increasing stratification and decreasing productivity was reported before and without relying on a causality-based approach (Lozier et al., 2011), PCMCI+ allows for the identification of models with changing dynamics. As hypothesized in (Bénard et al., 2025), ESMs lacking a negative link between stratification and net primary productivity under pre-industrial conditions may see an emerging link as climate change progresses. This is observed in CanESM5-CanOE and CMCC-ESM2 (Table 2). For CanESM5-CanOE, the evolution of the link strength under the different scenarios is illustrated in Figure 3. Across all the scenarios, the link deviates from the pre-industrial distribution in recent years, reaching a significant strength of approximately -0.4. The trend in the strength of this relationship, calculated from 1940 to the end of the simulation period, is between  $-4.5 \times 10^{-3}$  per year and  $-4.9 \times 10^{-3}$  per year depending on the scenario. CMCC-ESM2 exhibits a similar pattern across all scenarios, with a significant negative link between stratification and primary productivity outside the pre-industrial distribution, also reaching a strength of approximately -0.4 (Table 2). However, the evolution occurs more rapidly over a shorter period. The trend from 1940 to 1970 ranges from  $-1.25 \times 10^{-2}$  per year to  $-1.45 \times 10^{-2}$  per year depending on the scenario. The peak of strength is centred around 1980, and in the SSP126 scenario, values return inside the pre-industrial range during the final years.

In CanESM5-CanOE and CMCC-ESM2 climate change causes an increase in stratification along with a strengthening of the relationship between stratification and net primary productivity. Consequently, stratification becomes a crucial control for NPP in these models. Lastly, unchanged links are found for IPSL-CM6A-LR and CESM2. IPSL-CM6A-LR has a strong negative link and CESM2 has a low non-significant link both within their respective pre-industrial distribution.

**Table 2.** Summary of stratification-NPP relationships. Trend indicators, significance, and formatting are similar to Table 1. Values in brackets indicate the ranges observed for the three nutrients. NA indicates data not available.

| Model         | Trend    | Outside PI                               | Sig.                           | Intensity        |
|---------------|----------|--|--------------------------------|------------------|
| CanESM5-CanOE | //       | 35/[30-35]/[28-35]                       | [12-17]/[1-12]/[0-11]          | -0.35            |
| IPSL-CM6A-LR  | +/+/+    | 0/0/0                                    | 35/35/35                       | -0.6/-0.65/-0.65 |
| CMCC-ESM2     | //       | [0-12]/[1-18]/[2-30]                     | [0-30]/[7- <b>35</b> ]/[10-33] | -0.25/-0.3/-0.4  |
| CESM2         | ++/++/++ | NA                                       | 0/0/0                          | -                |
| UKESM1-0-LL   | -/-/-    | [26- <b>31</b> ]/[ <b>34-35</b> ]/[6-18] | 35/35/35                       | -0.75/-0.7/-0.7  |

For IPSL-CM6A-LR, the link between stratification  $\rightarrow$  and NPP is unchanged. It remains significant and strong (Table 2) between -0.6 and -0.65. Although this is comparable to the relationship observed in UKESM1-0-LL, underlying variables exhibit different trends in IPSL-CM6A-L. Under SSP285, the normalized trend for stratification is  $5 \times 10-3$  per year compared to a non significant NPP trend (Figure S5). The stronger trend in stratification suggests the presence of compensatory mechanisms that mitigate the expected negative impact of stratification on NPP. The maintenance of nutrient availability to fuel NPP





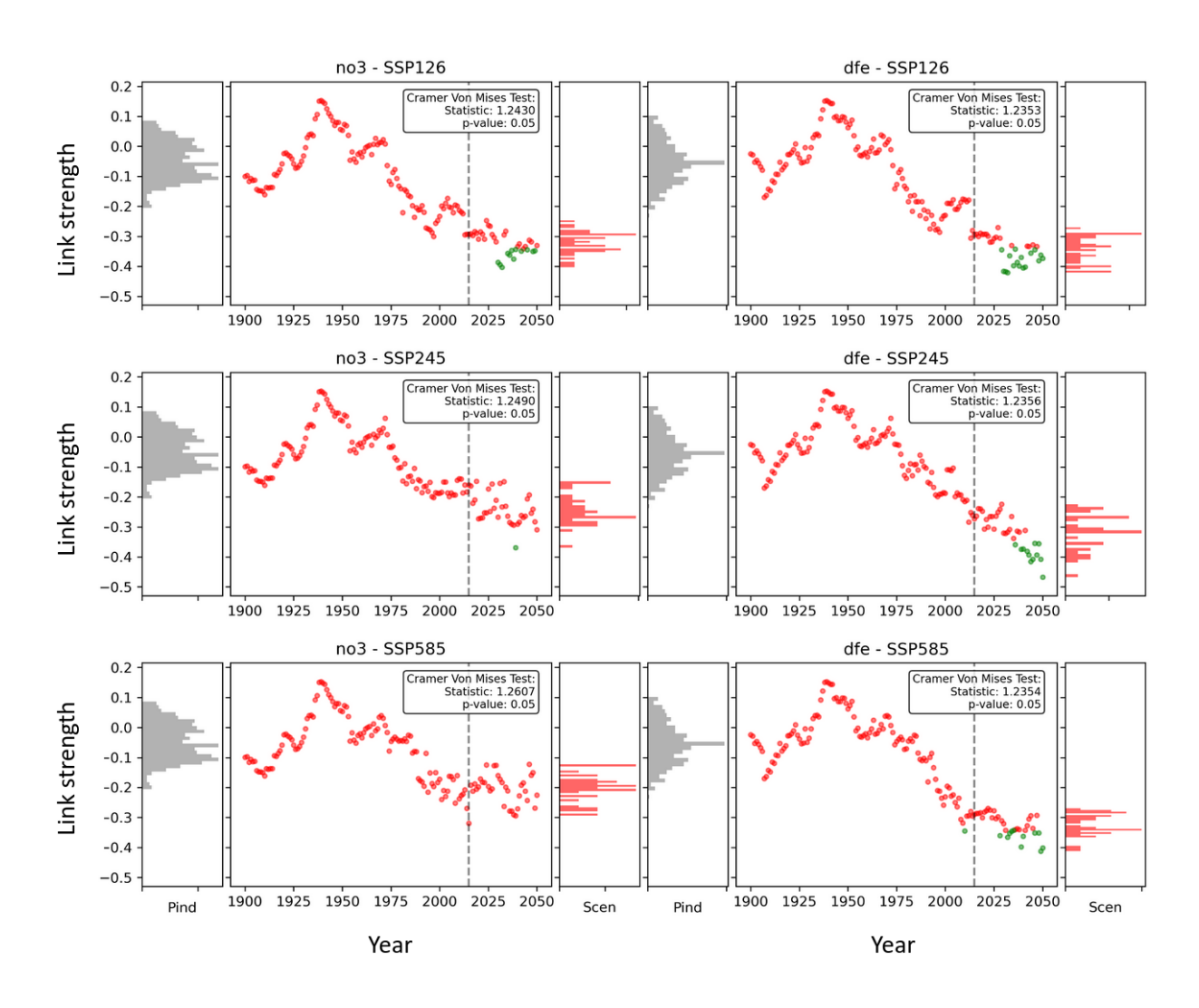


Figure 3. Similar to Figure 2 but for the link between stratification and NPP for CanESM5-CanOE.



260

265

275

280



appears to be the main explanation for this resilience. Indeed, the trends in nutrient concentrations under the SSP585 scenario remain relatively low and non-significant (between  $-1 \times 10-4$  and  $-7 \times 10-4$  depending on the nutrient, Figure S5). These trends are much closer to the NPP trend than to the stratification trend.

One of the main factors controlling nutrient concentrations is the variability of winter MLD. The results for the link MLD  $\rightarrow$  nutrient for all models are presented in Table 3. The CMCC-CESM2 exhibits an increase in strength for the link MLD  $\rightarrow$  nitrate and MLD  $\rightarrow$  silicate. From 1940 to the end we observe a significant trend ranging from  $2.6 \times 10^{-3}$  per year to  $2.95 \times 10^{-3}$  per year for nitrate and a significant trend ranging from  $3 \times 10^{-3}$  to  $3.5 \times 10^{-3}$  per year for silicate. In both cases, values outside of the pre-industrial range are reached: about 0.7 for nitrate and 0.8 for silicate (Table 3).

The CanESM5-CanOE shows a decreasing strength for the link MLD/nutrient reaching values out of the pre-industrial distribution for iron of approximately 0.6 (Table 3). The trend from 1980 to the end for the strength of the link between MLD and iron is at approximately  $-3 \times 10^{-3}$  per year. The MLD variability starts to lose control over iron concentration. For IPSL-CM6A-LR, the strength of the causal links also decreases over time. Negative trends are obtained over the entire period ranging between  $-1.2 \times 10^{-3}$  and  $-2.1 \times 10^{-3}$  per year for nitrate, silicate and phosphate, and between  $-3.3 \times 10^{-3}$ and  $-4.8 \times 10^{-3}$  for iron. However, as shown in Table 3, despite this weakening, the links remain significant and strong for most nutrients with strengths between 0.55 and 0.75 for nitrate, silicate and phosphate. For iron, the link is weaker (between 0.2 and 0.4). Winter MLD is shoaling in response to climate change with a strong trend of  $-4.5 \times 10^{-3}$  under SSP585. Given the causal links observed, nutrients should also be decreasing but the trends are not similar to MLD. The apparent weak control of stratification and winter MLD in IPSL-CM6A-LR on NPP is due to the compensation by horizontal transport bringing nutrients to the zone of study. In Figure 4, shows the evolution of the link strength for each nutrient and scenario. The relationship between horizontal transport and nutrient availability strengthens considerably. For nitrate, silicate and phosphate this relationship becomes significant in recent years, with values falling outside the pre-industrial range. The trend of the increase in link strength between 2020 and the end of the simulation ranges from  $3 \times 10^{-3}$  to  $9.5 \times 10^{-3}$  per year depending on the scenario and nutrient. For iron, although the link is not yet significant, a similar trend of approximately  $4.3 \times 10^{-3}$  per year is observed across all scenarios.

The transport mechanism begins to exert greater control over the distribution of nutrients distribution as climate change scenario unfolds. In the meantime the transport under SSP585 is increasing substantially (Figure S5). The combination of these two changes - an increase in transport rates and a strengthening relationship between transport and nutrients - can compensate for the impact of decreasing MLD and increasing stratification through the advection of nutrients with the gyre circulation in the IPSL-CM6A-LR.

This analysis reveals a shift in the dynamics of nutrient supply. While the winter mixing impact weakens, the role of horizontal transport in supplying nutrients gains prominence. This shift helps explain how nutrient availability can be maintained despite reduced vertical mixing, thereby moderating the expected decline in primary productivity under increased stratification.





**Table 3.** Similar to 1 but for the relationship between MLD and nutrients.

| Model         | Nutrient  | Trend    | Outside PI       | Sig.     | Intensity      |
|---------------|-----------|----------|------------------|----------|----------------|
|               | Nitrate   | -/-/-    | 21/12/25         | 34/35/35 | 0.55/0.60/0.60 |
| IPSL-CM6A-LR  | Silicate  | _/_/-    | 12/3/2           | 35/35/35 | 0.70/0.70/0.75 |
|               | Phosphate | _/_/_    | 14/11/6          | 34/35/35 | 0.55/0.60/0.60 |
|               | Iron      | _/_/_    | 35/35/35         | 19/0/35  | 0.35/0.20/0.40 |
|               | Nitrate   | ++/++/++ | 29/14/24         | 35/35/35 | 0.70/0.65/0.70 |
| CMCC-ESM2     | Silicate  | ++/++/++ | 35/35/33         | 35/35/35 | 0.80/0.80/0.75 |
|               | Phosphate | ++/++/++ | <b>35</b> /27/20 | 35/35/35 | 0.70/0.65/0.60 |
|               | Iron      | +/-/+    | 0/15/2           | 35/20/33 | 0.55/0.40/0.50 |
|               | Nitrate   | -/+/-    | 3/2/0            | 35/35/35 | 0.75/0.85/0.75 |
| CanESM5-CanOE | Iron      | -/-/-    | 23/31/32         | 35/35/35 | 0.70/0.70/0.70 |
|               | Nitrate   | -/-/-    | 0/0/0            | 35/35/35 | 0.45/0.50/0.50 |
| UKESM1-0-LL   | Silicate  | -/+/+    | 0/0/0            | 35/35/35 | 0.65/0.70/0.70 |
|               | Phosphate | -/-/-    | 0/0/0            | 35/35/35 | 0.45/0.50/0.50 |
|               | Iron      | ++/++/+  | 0/0/0            | 0/0/0    |                |
|               | Nitrate   | 0/-/-    | NA               | 35/35/35 | 0.80/0.70/0.75 |
| CESM2         | Silicate  | +/0/0    | NA               | 35/35/35 | 0.80/0.70/0.70 |
|               | Phosphate | -/-/-    | NA               | 35/35/35 | 0.75/0.75/0.75 |
|               | Iron      | +/-/0    | NA               | 35/20/35 | 0.65/0.35/0.50 |

# 4 Limitations and Discussion

# 4.1 Limitations

290

295

The choice of 100 years long sliding windows has consequences on the results obtained. Our methodology cannot capture the dynamics of short-term nutrient limitation or regime shifts occurring within a 100-year period. However, it enables the detection of long-term trends in nutrient limitation and their significance for NPP. For instance, the IPSL model exhibits substantial changes in silicate relationships with NPP, while nitrate shows smaller variations compared to pre-industrial conditions. Given that diatom production remains relatively stable in our study region for this model (not shown), these patterns do not reflect shifts in diatom abundance but rather indicate an increasing tendency for silicate to become limiting compared to pre-industrial conditions. This capability to identify which nutrients are becoming more or less limiting over centennial timescales represents a strength of our approach. It provides insights into the evolving role of each nutrient that complement other studies focusing on nutrient limitation patterns at smaller timescales. For example, Laufkötter et al. (2015) observes changes in nutrient limitation regimes in different ESMs by analysing 20-years period. Our 100-year sliding window approach represents a methodological compromise. On the one hand, preliminary tests (not shown) indicated that 100-year windows provide accurate link strengths. On the other hand, this window size faces challenges with the non-stationarity inherent to climate change scenarios.



305

310



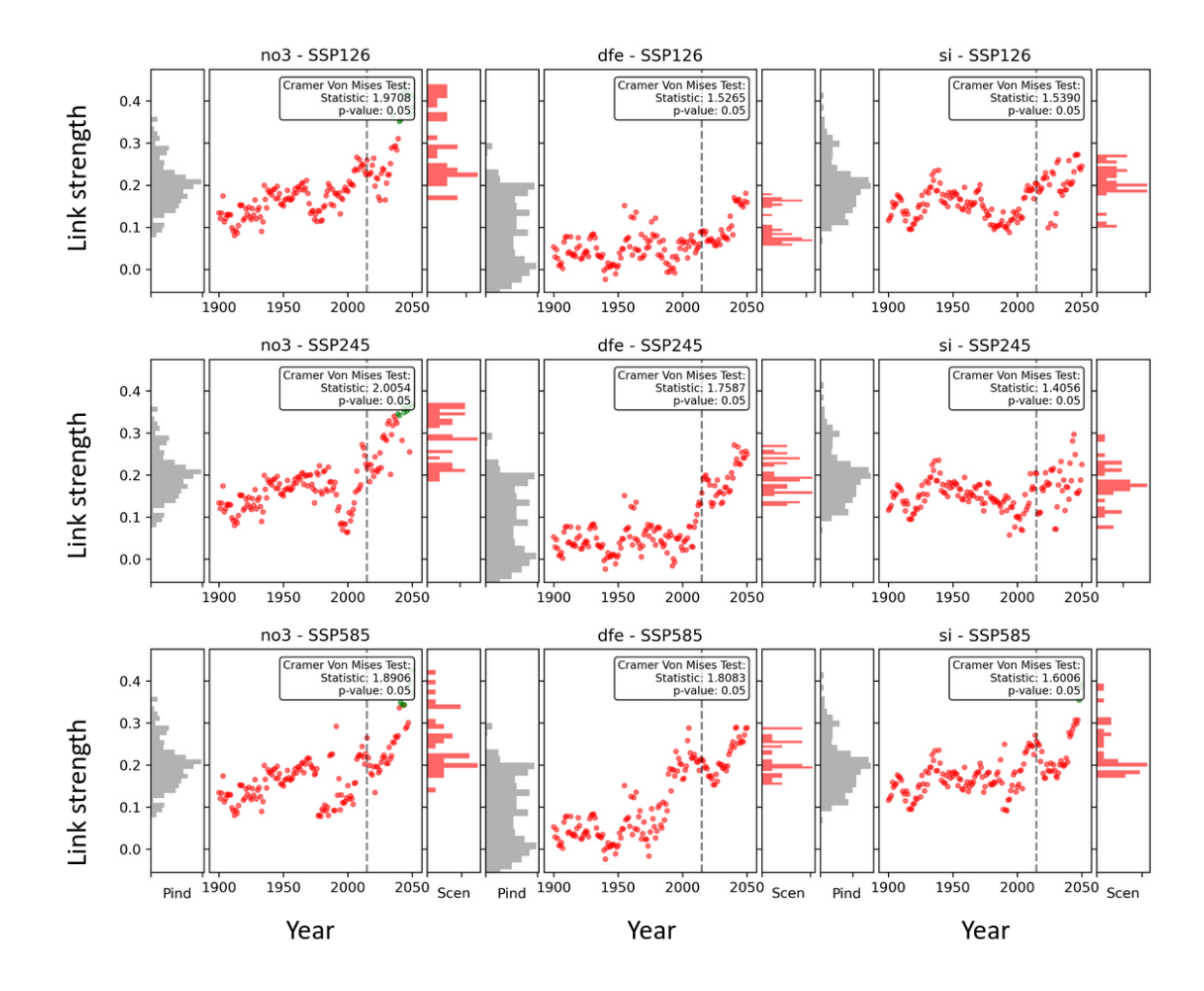


Figure 4. Similar to Figure 2 but for the link between transport and nutrient concentrations for IPSL-CM6A-LR.

As defined by Runge (2018), the stationarity required for causality analysis demands that conditional independence relationships between variables remain invariant over time. This definition is less restrictive than classical stationarity which requires stability in mean, variance, or spectral properties (Runge, 2018). However, in the context of climate change, even this weaker form of stationarity can be violated with anthropogenic forcing acting as a common non-stationary signal. This shared non-stationarity can lead to spurious links in the causal graph, as demonstrated by Runge (2018) (e.g., in the case of variables sharing a common trend). Our use of 100 years sliding windows aims to mitigate this issue by restricting the analysis to periods where non-stationarity is less pronounced and results from PCMCI+ are reliable. This choice can still be improved and especially on another point not mentioned by Runge (2018). If the interaction between two variables X and Y changes regime during the analyzed period, shifting for example from a relationship  $X = \alpha Y$  to  $X = \alpha' Y$ , our sliding window method will capture an intensity between  $\alpha$  and  $\alpha'$ . This value, while statistically robust, reflects neither the initial nor the final state of the





relationship. This characteristic is particularly well-suited for investigating long-term biogeochemical trends and century-scale shifts rather than transient fluctuations. Such an approach complements shorter-term studies by revealing whether observed changes represent temporary variability or sustained shifts in marine ecosystem dynamics.

# 4.2 Discussion

325

330

335

340

Understanding the impact of climate change on marine ecosystems requires both trend analysis and understanding of underlying dynamics. Looking at trends alone, without understanding changes in dynamics, provides an incomplete picture. Similarly, analyzing variables without quantifying their influence on other variables would limit our understanding of the impacts of climate change. Our causality analysis complements previous studies by identifying which environmental drivers lead to NPP changes and how their dynamics differ from pre-industrial conditions. For instance, while Tagliabue et al. (2021) could only suggest the drivers of a changing NPP (stratification, transport of nutrient), our analysis quantifies how the role of the nutrient transport evolves in IPSL-CM6A-LR.

The definition of transport through a fixed section at 33°W represents a methodological improvement compared to the approach used in Bénard et al. (2025), where integrated incoming fluxes to the area of study were considered. Our results show a stronger transport which aligns with the eastern current intensification identified by Sonnewald and Lguensat (2021).

This strengthening relationship creates a compensatory mechanism against the negative effects of increasing stratification. Indeed, the link "stratification  $\rightarrow$  NPP" is strong in IPSL-CM6A-LR. However, the emergence of this "transport  $\rightarrow$  nutrient" relationship helps moderate productivity declines, contrasting with models like UKESM1-0-LL where NPP strongly declines and the "stratification  $\rightarrow$  NPP" link dominates without apparent compensation.

The results concerning nutrient availability in IPSL-CM6A-LR also highlight fundamental limitations for the application of emergent constraints. Emergent constraints rely on the assumption that observable relationships in current climate remain valid predictors of future responses (Williamson et al., 2021). However, our results demonstrate that the causal mechanisms governing nutrient availability are non-stationary under climate change, with causal relationships that can emerge or disappear depending on the model. This finding reflects a broader issue with emergent constraints. Schlund et al. (2020) showed that emergent constraints derived from CMIP5 models largely failed when applied to CMIP6, with most constraints losing statistical significance. They attributed this degradation to the emergence of new feedback processes in more complex models that were not dominant in earlier generations. Similarly, our analysis reveals shifts in biogeochemical processes: transport mechanisms can become increasingly important for nutrient distributions while the influence of MLD decreases, though this transition varies across models.

The heterogeneous evolution of causal relationships between models suggests that the traditional emergent constraints approach might be inadequate for marine biogeochemical projections. Instead, a new generation of conditional emergent constraints should be developed, accounting for model-dependent shifts in causal mechanisms under climate change.

Concerning the link "stratification  $\rightarrow$  NPP", our analysis reveals a convergence of models toward a consensus under climate change. Models that initially exhibited weaker stratification-NPP links show increasing intensities over time, thereby narrowing the dispersion between model. This result is consistent with Fu et al. (2016) where stratification co-varies with NPP under



350

355

360

365

375



climate change in most of the ESMs studied. Moreover, our analysis reveals that the stratification-productivity is a smaller source of uncertainty compared to pre-industrial simulations, suggesting that enhanced stratification impacts represent a robust feature of future ocean productivity changes across the models.

In contrast to the consensus on stratification effects, the link "mixed layer depth → nutrients" shows a more dispersed evolution in reponse to climate change, with two models displaying weakening relationships and one intensification. This lack of agreement suggests that mixed layer dynamics represents a greater source of inter-model uncertainty compared to pre-industrial simulations. Similarly, nutrient relationships with NPP display comparable inconsistencies across models, with weakening and intensifying links. The role of nutrients for productivity and their source through mixed layer depth dynamics both exhibit dispersed evolution across models, representing a greater source of uncertainty compared to pre-industrial conditions.

Additional results not presented here also demonstrate the critical role of variable selection in developing the conceptual framework We identified the emergence of a link "NAO  $\rightarrow$  stratification" for CMCC-ESM2 and CESM2. The shared atmospheric component in CMCC-ESM2 and CESM2 likely drives their similar "NAO  $\rightarrow$  stratification" link, emerging as climate change progresses. This emergence may reflect the weakening of other stratification controls under climate change, making the NAO effect more apparent. By considering a more complete set of variables adapted to this specific question (e.g., temperature, salinity), Sallée et al. (2021) provides a deeper analysis of these stratification control mechanisms.

The emergence of such relationships with models sharing components raises the broader question of how common components between models influence their response to climate change. This behavioral similarity between models sharing components has been highlighted in several studies. Sittichok and Thepprasit (2022) and Lovato et al. (2022) identified commonalities between CMCC-ESM2 and CESM2 in other aspects of their climate forcing response. Our analysis confirms the relevance of such a comparative approach: not only do we observe similar responses from these two models in their atmospheric control of stratification, but we had also identified similarities in their behavior in (Bénard et al., 2025). These results align with Pan et al. (2023)'s recommendations, suggesting the importance of comparative analyses between groups of models sharing specific components.

# 5 Conclusion and Perspectives

## 5.1 Conclusion

Causal relationship analysis in the eastern subpolar North Atlantic under different climate change scenarios revealed significant evolutions in the mechanisms controlling primary productivity. Using 100-year sliding windows, systematically compared to pre-industrial variability, we identified three major types of changes in causal relationships: the emergence of new significant relationships, particularly visible in the stratification-productivity link, the strengthening of pre-existing connections, notably in nutrient-productivity relationships, and the weakening of established relationships (e.g. the MLD-nutrient link).

These modifications are heterogeneous, as shown in the evolution of nutrient supply mechanisms. The role of nutrients evolves distinctly across models, with notably increasing importance of nitrate in CanESM5-CanOE and silicate in IPSL-CM6A-LR. IPSL-CM6A-LR shows a marked transition from vertical mixing control to an enhanced role of horizontal trans-



380

385

395

400

405



port. This reorganization maintains nutrient availability despite weakening winter mixing. Conversely, CMCC-ESM2 exhibits strengthening mixed layer control over nitrate and silicate concentrations, with relationships reaching intensities exceeding the pre-industrial distribution. Finally, CanESM5-CanOE shows a weakening of mixed layer control without developing any apparent compensatory mechanism. This demonstrates a significant diversity in responses to climate forcing.

This diversity in the evolution of control mechanisms provides new insights into the origin of uncertainty in primary productivity projections for the eastern subpolar gyre. This region, identified by Tagliabue et al. (2021) as a region with high inter-model spread in projections, has its uncertainty partially explained by our causal analysis. Models respond to climate change through different mechanisms: some demonstrate the ability to maintain productivity through horizontal nutrient transport, while others see their biological production more directly constrained by increased stratification. This identification of different response pathways contributes to our understanding of the spread of model results in future projections and suggests avenues for model improvements.

# 5.2 Perspectives

This study opens several avenues for future research to deepen our understanding of NPP variability under climate change. While the role of subtropical waters as a source of nutrients has been discussed above, following Hátún et al. (2017)'s findings, analyzing other transports would provide a more complete picture of nutrient pathways in the eastern subpolar gyre.

Our analysis focused on total primary productivity, but examining different phytoplankton functional groups could provide deeper insights into community reorganization under climate change. ESMs selected for this study include at least two different phytoplankton functional types, allowing a first investigation of the responses of phytoplankton types to environmental drivers. This analysis could reveal compensatory mechanisms between functional groups that might maintain overall productivity despite community restructuring. Additionally, incorporating other key processes such as grazing pressure and light limitation could help explain inter-model differences in NPP projections.

Future studies would benefit from incorporating additional biological variables to refine our understanding of ecosystem responses. Doléac et al. (2025) demonstrates significant contributions of nitrate variability to diatoms and small phytoplankton production across different ocean regions (specifically for the model CESM2 and UKESM1-0-LL). In contrast, our analysis focusing on the eastern North Atlantic subpolar gyre (which is not considered in Doléac et al. (2025)) reveals a strong nitrate-total primary production relationship for UKESM1-0-LL but not for CESM2. This difference could be due to the aggregation of phytoplankton functional groups in our study: while Doléac et al. (2025) examines separate phytoplankton groups, the use of total NPP in the present study masks distinct responses of different functional groups. A causality analysis examining the "nitrate → small phytoplankton production" link would be particularly valuable to confirm whether CESM2's apparent insensitivity to nitrate variations reflects genuine model behavior or results from compensatory effects between different phytoplankton groups that become apparent only when analyzed separately.

Finally, the application of our causal methodology to observational data may be challenging due to data availability and the limitations of the methodology discussed in (Bénard et al., 2025). However such an application would provide valuable model evaluation opportunities and insights into the real-world dynamics.





Code availability. Analyses were performed using the Tigramite Python package: https://github.com/jakobrunge/tigramite (last access: 3 November 2025)).

Data availability. The CMIP6 model simulations can be downloaded through the Earth System Grid Federation portals. Instructions to access the data are available here: https://pcmdi.llnl.gov/CMIP6/Guide/dataUsers.html (last access: 3 November 2025).

*Author contributions.* All authors contributed to the development of the study, the interpretation of the results, and the writing of the manuscript. The lead author processed the data, obtained the results, and proposed the visualization of the results.

Competing interests. The authors declare that they have no conflict of interest

Acknowledgements. This study has been supported by the European Union's Horizon 2020 research and innovation program under grant agreement No. 862923 (project AtlantECO, Atlantic Ecosystems Assessment, Forecasting & Sustainability). This work has also been supported by the "COESION" project funded by the French National program LEFE (Les Enveloppes Fluides et l'Environnement). We acknowledge the World Climate Research Programme's Working Group on Coupled Modelling, which is responsible for CMIP, and we thank the climate modelling groups for producing and making available their model output.





#### References

430

- Anderson, T. W.: On the distribution of the two-sample Cramer-von Mises criterion, The Annals of Mathematical Statistics, pp. 1148–1159,
  - Behrenfeld, M. J., O'Malley, R. T., Siegel, D. A., McClain, C. R., Sarmiento, J. L., Feldman, G. C., Milligan, A. J., Falkowski, P. G., Letelier, R. M., and Boss, E. S.: Climate-driven trends in contemporary ocean productivity, Nature, 444, 752–755, 2006.
  - Bénard, G., Gehlen, M., and Vrac, M.: A causality-based method for multi-model comparison: application to relationships between atmospheric, oceanic and marine biogeochemical variables, Earth System Dynamics, 16, 1085–1102, 2025.
    - Benjamini, Y. and Hochberg, Y.: Controlling the false discovery rate: a practical and powerful approach to multiple testing, Journal of the Royal statistical society: series B (Methodological), 57, 289–300, 1995.
    - Bishop, S. P., Small, R. J., and Bryan, F. O.: The global sink of available potential energy by mesoscale air-sea interaction, Journal of Advances in Modeling Earth Systems, 12, e2020MS002 118, 2020.
- Bonan, G. and Doney, S.: Climate, ecosystems, and planetary futures: The challenge to predict life in Earth system models, Science, 359, eaam8328, 2018.
  - Bopp, L., Resplandy, L., Orr, J. C., Doney, S. C., Dunne, J. P., Gehlen, M., Halloran, P., Heinze, C., Ilyina, T., Seferian, R., et al.: Multiple stressors of ocean ecosystems in the 21st century: projections with CMIP5 models, Biogeosciences, 10, 6225–6245, 2013.
- Boucher, O., Servonnat, J., Albright, A. L., Aumont, O., Balkanski, Y., Bastrikov, V., Bekki, S., Bonnet, R., Bony, S., Bopp, L., Braconnot,
  P., Brockmann, P., Cadule, P., Caubel, A., Cheruy, F., Codron, F., Cozic, A., Cugnet, D., D'Andrea, F., Davini, P., de Lavergne, C., Denvil,
  S., Deshayes, J., Devilliers, M., Ducharne, A., Dufresne, J.-L., Dupont, E., Éthé, C., Fairhead, L., Falletti, L., Flavoni, S., Foujols, M.-A.,
  Gardoll, S., Gastineau, G., Ghattas, J., Grandpeix, J.-Y., Guenet, B., Guez, Lionel, E., Guilyardi, E., Guimberteau, M., Hauglustaine, D.,
  Hourdin, F., Idelkadi, A., Joussaume, S., Kageyama, M., Khodri, M., Krinner, G., Lebas, N., Levavasseur, G., Lévy, C., Li, L., Lott, F.,
  Lurton, T., Luyssaert, S., Madec, G., Madeleine, J.-B., Maignan, F., Marchand, M., Marti, O., Mellul, L., Meurdesoif, Y., Mignot, J., Musat,
- 445 I., Ottlé, C., Peylin, P., Planton, Y., Polcher, J., Rio, C., Rochetin, N., Rousset, C., Sepulchre, P., Sima, A., Swingedouw, D., Thiéblemont, R., Traore, A. K., Vancoppenolle, M., Vial, J., Vialard, J., Viovy, N., and Vuichard, N.: Presentation and Evaluation of the IPSL-CM6A-LR Climate Model, Journal of Advances in Modeling Earth Systems, 12, e2019MS002 010, https://doi.org/10.1029/2019MS002010, 2020.
  - Brody, S. R., Lozier, M. S., and Dunne, J. P.: A comparison of methods to determine phytoplankton bloom initiation, Journal of Geophysical Research: Oceans, 118, 2345–2357, 2013.
- 450 Christian, J. R., Denman, K. L., Hayashida, H., Holdsworth, A. M., Lee, W. G., Riche, O. G., Shao, A. E., Steiner, N., and Swart, N. C.: Ocean biogeochemistry in the canadian earth system model version 5.0. 3: CanESM5 and CanESM5-CanOE, Geoscientific Model Development Discussions, 2021, 1–68, 2021.
  - Damerell, G. M., Heywood, K. J., Calvert, D., Grant, A. L., Bell, M. J., and Belcher, S. E.: A comparison of five surface mixed layer models with a year of observations in the North Atlantic, Progress in Oceanography, 187, 102 316, 2020.
- Danabasoglu, G., Lamarque, J.-F., Bacmeister, J., Bailey, D. A., DuVivier, A. K., Edwards, J., Emmons, L. K., Fasullo, J., Garcia, R., Gettelman, A., Hannay, C., Holland, M. M., Large, W. G., Lauritzen, P. H., Lawrence, D. M., Lenaerts, J. T. M., Lindsay, K., Lipscomb, W. H., Mills, M. J., Neale, R., Oleson, K. W., Otto-Bliesner, B., Phillips, A. S., Sacks, W., Tilmes, S., van Kampenhout, L., Vertenstein, M., Bertini, A., Dennis, J., Deser, C., Fischer, C., Fox-Kemper, B., Kay, J. E., Kinnison, D., Kushner, P. J., Larson, V. E., Long, M. C., Mickelson, S., Moore, J. K., Nienhouse, E., Polvani, L., Rasch, P. J., and Strand, W. G.: The Community Earth System Model Version 2
  (CESM2), Journal of Advances in Modeling Earth Systems, 12, e2019MS001916, https://doi.org/10.1029/2019MS001916, 2020.



465

470

485



- Doléac, S., Lévy, M., El Hourany, R., and Bopp, L.: Toward more robust net primary production projections in the North Atlantic Ocean, Biogeosciences, 22, 841–862, 2025.
- D'Asaro, E. A.: Convection and the seeding of the North Atlantic bloom, Journal of Marine Systems, 69, 233-237, 2008.
- Fu, W., Randerson, J. T., and Moore, J. K.: Climate change impacts on net primary production (NPP) and export production (EP) regulated by increasing stratification and phytoplankton community structure in the CMIP5 models, Biogeosciences, 13, 5151–5170, 2016.
- Hátún, H., Azetsu-Scott, K., Somavilla, R., Rey, F., Johnson, C., Mathis, M., Mikolajewicz, U., Coupel, P., Tremblay, J.-É., Hartman, S., et al.: The subpolar gyre regulates silicate concentrations in the North Atlantic, Scientific reports, 7, 14576, 2017.
- Holliday, N. P., Bersch, M., Berx, B., Chafik, L., Cunningham, S., Florindo-López, C., Hátún, H., Johns, W., Josey, S. A., Larsen, K. M. H., et al.: Ocean circulation causes the largest freshening event for 120 years in eastern subpolar North Atlantic, Nature communications, 11, 585, 2020.
- Hurrell, J., Kushnir, Y., Ottersen, G., and Visbeck, M.: An overview of the North Atlantic Oscillation, vol. 134, pp. 1–36, 2003a.
- Hurrell, J. W., Kushnir, Y., Ottersen, G., and Visbeck, M.: An overview of the North Atlantic oscillation, Geophysical Monograph-American Geophysical Union, 134, 1–36, 2003b.
- Khatri, H., Williams, R. G., Woollings, T., and Smith, D. M.: Fast and slow subpolar ocean responses to the North Atlantic Oscillation:

  Thermal and dynamical changes, Geophysical Research Letters, 49, e2022GL101480, 2022.
  - Kim, T. K.: T test as a parametric statistic, Korean journal of anesthesiology, 68, 540–546, 2015.
  - Kwiatkowski, L., Torres, O., Bopp, L., Aumont, O., Chamberlain, M., Christian, J. R., Dunne, J. P., Gehlen, M., Ilyina, T., John, J. G., et al.: Twenty-first century ocean warming, acidification, deoxygenation, and upper-ocean nutrient and primary production decline from CMIP6 model projections, Biogeosciences, 17, 3439–3470, 2020.
- Large, W. and Yeager, S.: On the observed trends and changes in global sea surface temperature and air–sea heat fluxes (1984–2006), Journal of Climate, 25, 6123–6135, 2012.
  - Laufkötter, C., Vogt, M., Gruber, N., Aita-Noguchi, M., Aumont, O., Bopp, L., Buitenhuis, E., Doney, S. C., Dunne, J., Hashioka, T., Hauck, J., Hirata, T., John, J., Le Quéré, C., Lima, I. D., Nakano, H., Seferian, R., Totterdell, I., Vichi, M., and Völker, C.: Drivers and uncertainties of future global marine primary production in marine ecosystem models, Biogeosciences, 12, 6955–6984, https://doi.org/10.5194/bg-12-6955-2015, 2015.
  - Lovato, T., Peano, D., Butenschön, M., Materia, S., Iovino, D., Scoccimarro, E., Fogli, P., Cherchi, A., Bellucci, A., Gualdi, S., et al.: CMIP6 simulations with the CMCC Earth system model (CMCC-ESM2), Journal of Advances in Modeling Earth Systems, 14, e2021MS002814, 2022.
- Lozier, M. S., Dave, A. C., Palter, J. B., Gerber, L. M., and Barber, R. T.: On the relationship between stratification and primary productivity in the North Atlantic, Geophysical Research Letters, 38, 2011.
  - Martinez, E., Antoine, D., d'Ortenzio, F., and de Boyer Montégut, C.: Phytoplankton spring and fall blooms in the North Atlantic in the 1980s and 2000s, Journal of geophysical research: oceans, 116, 2011.
  - Pan, R., Shu, Q., Wang, Q., Wang, S., Song, Z., He, Y., and Qiao, F.: Future Arctic climate change in CMIP6 strikingly intensified by nemo-family climate models, Geophysical Research Letters, 50, e2022GL102077, 2023.
- Pelegrí, J. L., Marrero-Díaz, A., and Ratsimandresy, A.: Nutrient irrigation of the North Atlantic, Progress in Oceanography, 70, 366–406, 2006.





- Riahi, K., Van Vuuren, D. P., Kriegler, E., Edmonds, J., O'neill, B. C., Fujimori, S., Bauer, N., Calvin, K., Dellink, R., Fricko, O., et al.: The Shared Socioeconomic Pathways and their energy, land use, and greenhouse gas emissions implications: An overview, Global environmental change, 42, 153–168, 2017.
- 500 Rossby, T.: The North Atlantic Current and surrounding waters: At the crossroads, Reviews of Geophysics, 34, 463–481, 1996.
  - Runge, J.: Causal network reconstruction from time series: From theoretical assumptions to practical estimation, Chaos: An Interdisciplinary Journal of Nonlinear Science, 28, 2018.
  - Runge, J.: Discovering instantaneous and lagged causal relations in autocorrelated nonlinear time series datasets, 2020.
- Runge, J., Nowack, P., Kretschmer, M., Flaxman, S., and Sejdinovic, D.: Detecting and quantifying causal associations in large nonlinear time series datasets, Science advances, 5, eaau4996, 2019.
  - Sallée, J.-B., Pellichero, V., Akhoudas, C., Pauthenet, E., Vignes, L., Schmidtko, S., Garabato, A. N., Sutherland, P., and Kuusela, M.: Summertime increases in upper-ocean stratification and mixed-layer depth, Nature, 591, 592–598, 2021.
  - Schlund, M., Lauer, A., Gentine, P., Sherwood, S. C., and Eyring, V.: Emergent constraints on equilibrium climate sensitivity in CMIP5: do they hold for CMIP6?, Earth System Dynamics, 11, 1233–1258, 2020.
- 510 Séférian, R., Berthet, S., Yool, A., Palmiéri, J., Bopp, L., Tagliabue, A., Kwiatkowski, L., Aumont, O., Christian, J., Dunne, J., et al.: Tracking improvement in simulated marine biogeochemistry between CMIP5 and CMIP6, Current Climate Change Reports, 6, 95–119, 2020.
  - Sellar, A. A., Jones, C. G., Mulcahy, J. P., Tang, Y., Yool, A., Wiltshire, A., O'Connor, F. M., Stringer, M., Hill, R., Palmieri, J., Woodward, S., de Mora, L., Kuhlbrodt, T., Rumbold, S. T., Kelley, D. I., Ellis, R., Johnson, C. E., Walton, J., Abraham, N. L., Andrews, M. B., Andrews, T., Archibald, A. T., Berthou, S., Burke, E., Blockley, E., Carslaw, K., Dalvi, M., Edwards, J., Folberth, G. A., Gedney, N.,
- Griffiths, P. T., Harper, A. B., Hendry, M. A., Hewitt, A. J., Johnson, B., Jones, A., Jones, C. D., Keeble, J., Liddicoat, S., Morgenstern, O., Parker, R. J., Predoi, V., Robertson, E., Siahaan, A., Smith, R. S., Swaminathan, R., Woodhouse, M. T., Zeng, G., and Zerroukat, M.: UKESM1: Description and Evaluation of the U.K. Earth System Model, Journal of Advances in Modeling Earth Systems, 11, 4513–4558, https://doi.org/10.1029/2019MS001739, 2019.
- Sittichok, K. and Thepprasit, C.: The Differences of Precipitation Characteristics among GCMs over Southeast Asia under AR6 Climate

  Change Scenarios, ASEAN Journal of Scientific and Technological Reports, 25, 11–23, 2022.
  - Sonnewald, M. and Lguensat, R.: Revealing the impact of global heating on North Atlantic circulation using transparent machine learning, Journal of Advances in Modeling Earth Systems, 13, e2021MS002 496, 2021.
  - Steinhoff, T., Friedrich, T., Hartman, S., Oschlies, A., Wallace, D. W., and Körtzinger, A.: Estimating mixed layer nitrate in the North Atlantic Ocean, Biogeosciences, 7, 795–807, 2010.
- Swart, N. C., Cole, J. N. S., Kharin, V. V., Lazare, M., Scinocca, J. F., Gillett, N. P., Anstey, J., Arora, V., Christian, J. R., Hanna, S., Jiao, Y., Lee, W. G., Majaess, F., Saenko, O. A., Seiler, C., Seinen, C., Shao, A., Sigmond, M., Solheim, L., von Salzen, K., Yang, D., and Winter, B.: The Canadian Earth System Model version 5 (CanESM5.0.3), Geoscientific Model Development, 12, 4823–4873, https://doi.org/10.5194/gmd-12-4823-2019, 2019.
- Tagliabue, A., Kwiatkowski, L., Bopp, L., Butenschön, M., Cheung, W., Lengaigne, M., and Vialard, J.: Persistent uncertainties in ocean net
   primary production climate change projections at regional scales raise challenges for assessing impacts on ecosystem services, Frontiers in Climate, 3, 2021.
  - Tsujino, H., Urakawa, L. S., Griffies, S. M., Danabasoglu, G., Adcroft, A. J., Amaral, A. E., Arsouze, T., Bentsen, M., Bernardello, R., Böning, C. W., et al.: Evaluation of global ocean–sea-ice model simulations based on the experimental protocols of the Ocean Model Intercomparison Project phase 2 (OMIP-2), Geoscientific Model Development, 13, 3643–3708, 2020.





- Turnock, S. T., Allen, R. J., Andrews, M., Bauer, S. E., Deushi, M., Emmons, L., Good, P., Horowitz, L., John, J. G., Michou, M., et al.: Historical and future changes in air pollutants from CMIP6 models, Atmospheric Chemistry and Physics, 20, 14547–14579, 2020.
  - Ukkola, A. M., De Kauwe, M. G., Roderick, M. L., Abramowitz, G., and Pitman, A. J.: Robust future changes in meteorological drought in CMIP6 projections despite uncertainty in precipitation, Geophysical Research Letters, 47, e2020GL087 820, 2020.
- Vautard, R., Kadygrov, N., Iles, C., Boberg, F., Buonomo, E., Bülow, K., Coppola, E., Corre, L., van Meijgaard, E., Nogherotto, R., et al.: Evaluation of the large EURO-CORDEX regional climate model ensemble, Journal of Geophysical Research: Atmospheres, 126, e2019JD032 344, 2021.
  - Whitt, D. B. and Jansen, M. F.: Slower nutrient stream suppresses Subarctic Atlantic Ocean biological productivity in global warming, Proceedings of the National Academy of Sciences, 117, 15504–15510, 2020.
- Williams, R. G., Roussenov, V., and Follows, M. J.: Nutrient streams and their induction into the mixed layer, Global Biogeochemical Cycles, 20, 2006.
  - Williams, R. G., McDonagh, E., Roussenov, V. M., Torres-Valdes, S., King, B., Sanders, R., and Hansell, D. A.: Nutrient streams in the North Atlantic: Advective pathways of inorganic and dissolved organic nutrients, Global Biogeochemical Cycles, 25, 2011.
  - Williamson, M. S., Thackeray, C. W., Cox, P. M., Hall, A., Huntingford, C., and Nijsse, F. J.: Emergent constraints on climate sensitivities, Reviews of Modern Physics, 93, 025 004, 2021.
- Yool, A., Palmiéri, J., Jones, C. G., de Mora, L., Kuhlbrodt, T., Popova, E. E., Nurser, A. J. G., Hirschi, J., Blaker, A. T., Coward, A. C., Blockley, E. W., and Sellar, A. A.: Evaluating the physical and biogeochemical state of the global ocean component of UKESM1 in CMIP6 historical simulations, https://doi.org/10.5194/gmd-14-3437-2021, 2021.
  - Zelinka, M. D., Myers, T. A., McCoy, D. T., Po-Chedley, S., Caldwell, P. M., Ceppi, P., Klein, S. A., and Taylor, K. E.: Causes of higher climate sensitivity in CMIP6 models, Geophysical Research Letters, 47, e2019GL085782, 2020.